Polarized and compartment-dependent distribution of HCN1 in pyramidal cell dendrites

Andrea Lörincz[1,2], Takuya Notomi[3], Gábor Tamás[2], Ryuichi Shigemoto[3] and Zoltan Nusser[1]

[1]*Laboratory of Cellular Neurophysiology, Institute of Experimental Medicine, Hungarian Academy of Sciences Szigony Street 43, 1083 Budapest, Hungary*

[2]*Department of Comparative Physiology, University of Szeged, Közép fasor 52, 6726 Szeged, Hungary*

[3]*Division of Cerebral Structure, National Institute for Physiological Sciences, The Graduate University for Advanced Studies, School of Life Science, Okazaki, CREST Japan Science and Technology Corporation, Kawaguchi,Okazaki 444-8585, Japan*

Correspondence should be addressed to Z.N. (nusser@koki.hu)

Published online 21 October 2002; doi:10.1038/nn962

An ion channel's function depends largely on its location and density on neurons. Here we used high-resolution immunolocalization to determine the subcellular distribution of the hyperpolarization-activated and cyclic-nucleotide-gated channel subunit 1 (HCN1) in rat brain. Light microscopy revealed graded HCN1 immunoreactivity in apical dendrites of hippocampal, subicular and neocortical layer-5 pyramidal cells. Quantitative comparison of immunogold densities showed a 60-fold increase from somatic to distal apical dendritic membranes. Distal dendritic shafts had 16 times more HCN1 labeling than proximal dendrites of similar diameters. At the same distance from the soma, the density of HCN1 was significantly higher in dendritic shafts than in spines. Our results reveal the complex cell surface distribution of voltage-gated ion-channels, and predict its role in increasing the computational power of single neurons via subcellular domain and input-specific mechanisms.

Ligand- and voltage-gated ion channels are fundamental building blocks of excitable nerve cells. The molecular diversity of these channels contributes to their functional heterogeneity[1]. However, not only the molecular structure but also the precise subcellular location and the density of channels are crucial in neuronal communication and integration[2–8]. The organizational principles of the cell-surface expression of ligand-gated ion channels have been studied. For example, high-resolution immunolocalization showed that AMPA-type[9–11] and NMDA-type[11–13] glutamate receptor subunits and $GABA_A$ receptor subunits[12,14,15] are selectively targeted to functionally different synapses of a single cell, establishing a presynaptic input-selective distribution of postsynaptic receptors. The amount and density of postsynaptic $GABA_A$ and glutamate receptors are also regulated in a presynaptic input-specific manner[10,11,16,17]. Furthermore, distinct $GABA_A$ receptor subtypes are segregated to synaptic versus extrasynaptic sites, underlying distinct forms of inhibition in certain cell types[18].

Much less is known about the cell-surface distribution of voltage-gated channels, although they are important in neuronal integration[5,8]. This is mainly due to the scarcity of high-resolution immunogold localization studies of these channels. Electron microscopic (EM) immunogold localization of voltage- and Ca^{2+}-activated K^+ channels (BK) showed their enrichment in presynaptic active zones of glutamatergic terminals and the lack of labeling on postsynaptic dendrites[19]. Voltage-gated channels on the axo-somato-dendritic surface of nerve cells have been mapped with patch-clamp recordings. This technique is extremely useful because it reveals the location of functional channels. However, small subcellular compartments remain inaccessible with this approach, and a differential current density does not necessarily mean distinct densities of channels. Patch-clamp studies suggested uneven subcellular distribution of transient A-type K^+ channels (I_A)[20], N-type Ca^{2+} channels[21,22], Na^+ channels[23,24] and hyperpolarization-activated channels in nerve cells[25–31], but a uniform density of Na^+ channels in the axo-somato-dendritic domains of some other cells was also reported[32,33]. The differential somato-dendritic distribution of I_A may not necessarily reflect a differential channel distribution, as these channels are differentially regulated by PKA and PKC across the somato-dendritic surface of hippocampal pyramidal cells[34]. Furthermore, all of these channels/currents have been recorded in large-diameter apical dendrites, but their density in small-diameter secondary dendrites and in spines remains elusive.

Here we used electron microscopy with immunogold localization of HCN1 to reveal its cell-surface distribution. HCN1 is one of the four known subunits (HCN1–4) of the hyperpolarization-activated and cyclic-nucleotide-gated nonselective cation channels[35–38]. The homo- or heteromeric assemblies of these subunits are mainly responsible for the functional diversities of H current (I_h)[39,40]. Our results demonstrate that this channel is unevenly distributed in the axo-somato-dendritic surface of pyramidal cells. The distal dendritic shafts had ~60-fold larger immunoparticle densities than the somata, whereas pyramidal cell axons were immunonegative. There was also a ~16-fold difference in the density of HCN1 label-

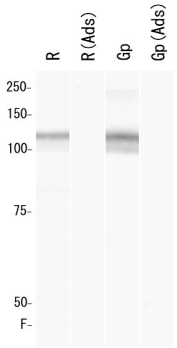

Fig. 1. Immunoblot analysis of rat brain with HCN1 antibodies. Crude membrane preparations from whole rat brains were reacted with HCN1 antibodies raised in a rabbit (R) and a guinea pig (Gp). No immunoreactivity is detected after adsorption of these antibodies with the corresponding antigens (Ads). Molecular mass markers (Bio-Rad) are indicated on the left in kDa. F, gel front.

ing between small-diameter distal and proximal dendrites. Moreover, distal dendritic shafts had ~4 times larger immunoreactive HCN1 densities than spines at the same distance from the soma, revealing a distance- and subcellular domain–specific regulation of the plasma membrane density of HCN1.

Results

HCN1 immunoreactivity in neocortex and hippocampus

The regional, cellular and subcellular distribution of HCN1 was investigated with two polyclonal antibodies (rabbit, HCN1-R; guinea pig, HCN1-Gp) directed against different, non-overlapping parts of the protein (Methods). The specificity of the rabbit and guinea pig antibodies was verified by immunoblot analysis of crude membrane fractions prepared from adult rat brains (**Fig. 1**). Both antibodies gave a broad immunoreactive band around a molecular mass of 120 kDa, consistent with a previous study[36].

The regional and cellular distribution of HCN1 immunostaining as revealed with the two antibodies was almost identical (**Figs. 2** and **3**), demonstrating that the immunolabeling is due to a specific antibody–antigen (HCN1) recognition. In the neocortex, bundles of strongly immunopositive apical dendrites of pyramidal cells were observed at the border of layers 3 and 4 (**Fig. 2**). The labeling intensity of the apical dendrites increased toward layer 1, with dendritic tufts showing the strongest labeling (**Fig. 2b** and **e**). These dendrites did not contain the calcium-binding protein calbindin D-28K, suggesting that they do not belong to layer-2/3 pyramidal cells (data not shown). The large diameter and the appearance of some of these apical dendrites already in layer 4 indicate that they belong to layer-5 pyramidal cells. Higher magnifications revealed that the strong immunoreactivity of the apical dendrites mainly originated from strong labeling of the plasma membrane (**Fig. 2c** and **f**). They appeared as tubes with apparently immunonegative cytoplasm surrounded by strongly labeled plasma membranes. Furthermore, dendritic spines emerging from these apical dendrites were also immunopositive in the upper layers (**Figs. 2c** and **f** and **3c** and **3d**). These data obtained at the light microscopic (LM) level are consistent with an increased density of HCN1 in the dendrites of layer-5 pyramidal cell as a function of distance from the soma. Punctate, relatively weak immunostaining of the neuropil was observed in all layers, the somata of nerve cells and the cytoplasm of large diameter dendrites being apparently immunonegative. The staining of the neu-

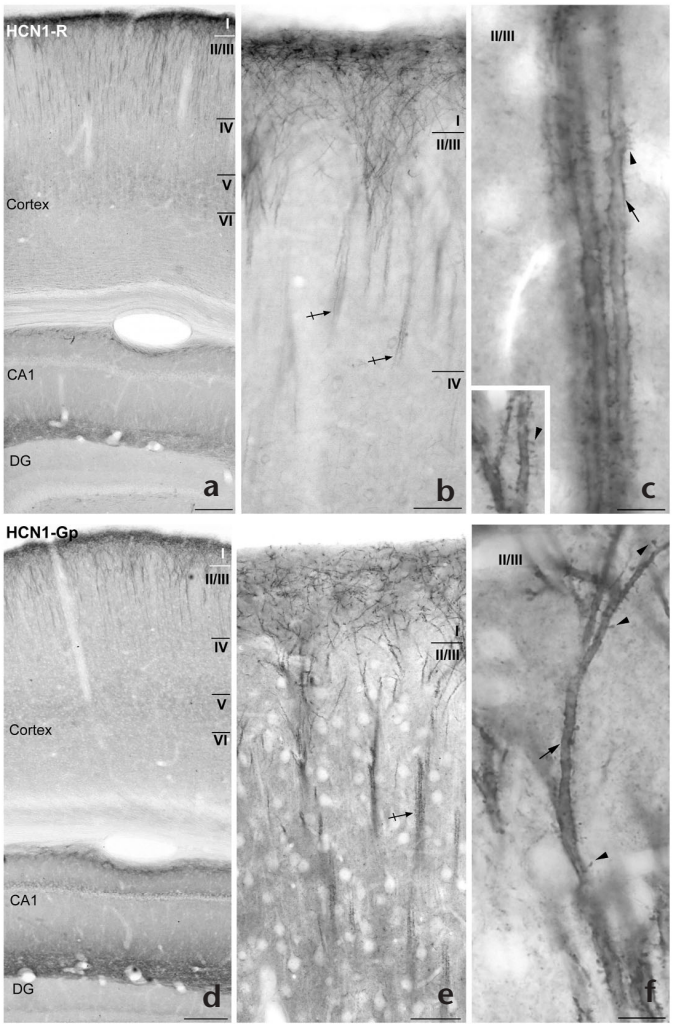

Fig. 2. Light microscopic demonstration of HCN1 immunoreactivity in rat neocortex. (**a**–**c**) HCN1-R antibodies. (**d**–**f**) HCN1-Gp antibodies. (**a**, **d**) Low-magnification images of the neocortex and hippocampus. Immunoreactivity is very similar with the two antibodies. Immunoreactive processes are seen in neocortical superficial layers. (**b**, **e**) Strongly HCN1 immunoreactive apical dendrites of layer-5 pyramidal cells appear in layer 3 (crossed arrows). The strength of reactivity increases toward the apical tufts. Neuropil labeling is stronger with the HCN1-Gp antibody. Note the immunonegativity of the cell bodies. (**c**, **f**) Higher-magnification view of the apical dendrites of layer-5 pyramidal cells. Immunoreactivity is associated with the dendritic plasma membrane (arrows). Dendritic spines (arrowheads) are also labeled (inset). DG, dentate gyrus. Scale bars, (**a**, **d**) 200 μm; (**b**, **e**) 50 μm; (**c**, **f**) 10 μm.

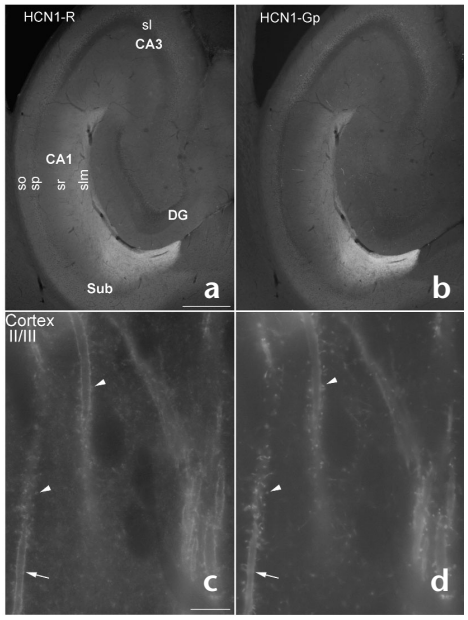

Fig. 3. Double-immunofluorescence labeling of HCN1 with the rabbit (left) and guinea pig (right) antibodies in hippocampus (**a**, **b**) and somatosensory cortex (**c**, **d**). Identical HCN1 labeling patterns are shown by the two antibodies. (**a**, **b**) The strongest immunolabeling is detected in the subiculum (Sub), followed by area CA1, area CA3, and the dentate gyrus (DG). In CA1, the intensity of immunolabeling increases from stratum pyramidale (sp) to stratum lacunosum-moleculare (slm). No detectable immunolabeling is seen in stratum lucidum (sl) of CA3 or in the granule cell layer of the dentate gyrus. Weak immunofluorescent signal is found in stratum pyramidale of CA1 and CA3. (**c**, **d**) High-magnification images of layer 2/3 of the somatosensory cortex. HCN1 immunolabeling outlines the distal apical dendrites (arrows) and spines (arrowheads) of layer-5 pyramidal cells, indicating that most immunoreactive HCN1 is present in the plasma membrane. sr, stratum radiatum; so, stratum oriens. Scale bars, (**a**, **b**) 400 μm; (**c**, **d**) 10 μm.

ropil was stronger with the HCN1-Gp antibody (**Fig. 2b** and **e**), which provided a somewhat stronger staining of all positive structures. This low-intensity neuropil labeling may be due to the weak staining of small-diameter secondary/tertiary dendrites, dendritic spines, axons/axon terminals or glial processes, or any combination of the above.

The stratum moleculare of the subiculum was the strongest subregion of the hippocampal formation, followed by the stratum lacunosum-moleculare of the CA1 area (**Fig. 3a** and **b**). The stratum lucidum of the CA3 area was immunonegative for HCN1; the cell body layers of all hippocampal regions showed moderate labeling of presumably inhibitory axon terminals. In CA1, the intensity of immunolabeling increased from the stratum pyramidale to the stratum lacunosum-moleculare. This pattern of labeling was observed with both immunoperoxidase (**Fig. 2**) and immunofluorescence (**Fig. 3**) methods, as were all LM findings of this study. As in the neocortex, intense labeling of the plasma membrane of the apical dendrites of CA1 and subicular pyramidal cells was observed at high magnifications. Some hippocampal interneurons also showed intense immunolabeling for HCN1. The identification of the cells and the precise subcellular distribution of HCN1 in these cells were outside the scope of the present study.

As the cell bodies of the CA1 pyramidal cells are nicely arranged in a single well defined layer, the stratum pyramidale, pyramidal cell dendrites and spines in any given segment of the strata radiatum and lacunosum-moleculare are approximately the same distance away from their parent somata. This arrangement allowed us to evaluate possible changes in the immunolabeling intensity as a function of distance from the soma at the light microscopic level. The highest intensity of HCN1 labeling was detected in the stratum lacunosum-moleculare, followed by the stratum radiatum and then the stratum oriens, with the lowest intensity in the stratum pyramidale. Within stratum radiatum, an increased labeling intensity was apparent toward the stratum lacunosum-moleculare. The most parsimonious explanation of the increase in immunofluorescent intensity is that the density of HCN1 in the plasma membrane of CA1 pyramidal cells dendrites increases as a function of distance from the soma. However, the contribution of a higher relative plasma membrane fraction of the tissue in the stratum lacunosum-moleculare could not be excluded based on light microscopic data. To determine whether the increased immunostaining of distal dendritic regions was indeed the consequence of a higher immunoreactive HCN1 density in distal dendrites, we used EM immunogold localization of HCN1 in these brain regions.

Subcellular distribution of HCN1 in pyramidal cells

First, we investigated the subcellular distribution of HCN1 in the neocortex (somatosensory) using EM immunoperoxidase and immunogold methods with both anti-HCN1 antibodies. Strongly immunopositive apical dendrites and dendritic spines of pyramidal cells dominated the upper cortical layers. Peroxidase reaction product covered the cytoplasm of apical dendrites and spines. No detectable staining was observed in glial processes, in glutamatergic axon terminals and in the cell bodies of neurons in the upper layers. Electron microscopic analysis demonstrated that most immunogold particles for HCN1 were attached to plasma membranes of apical dendrites and dendritic tufts in upper layers (**Fig. 4a** and **b**). Gold particles were found at the intracellular face of the membranes, in agreement with the intracellular location of the epitopes recognized by our antibodies. The density of HCN1 on the somata and proximal apical dendrites of layer-5 pyramidal cells was below the detection limit of our method. In neocortical pyramidal cells and all other studied cells (CA1 and subicular pyramidal cells), gold particles were not concentrated around asymmetrical synapses on dendritic spines, but were randomly distributed on the extrasynaptic membrane. Similarly, no elevated labeling was found in the vicinity of GABAergic synapses on dendritic shafts. Both glutamatergic and GABAergic synaptic junctions were always immunonegative with the pre-embedding immunogold method; however, this method does not allow us to conclude that the lack of labeling is indeed due to the lack of protein in synaptic junctions[41,42]. Despite our repeated efforts to localize HCN1 with a postembedding immunogold method, no specific labeling could be obtained with our current technique and antibodies. Thus, it remains to be seen whether HCN1 is indeed located exclusively outside the synaptic junctions.

We observed a pattern of labeling in the CA1 area very similar to that of the neocortex. The plasma membranes of distal dendrites of pyramidal cells were strongly outlined by immunoparticles. In the stratum lacunosum-moleculare, dendritic spines also contained detectable levels of HCN1 immunoreactivity, but at a lower density than in shafts (**Fig. 4c** and **d**).

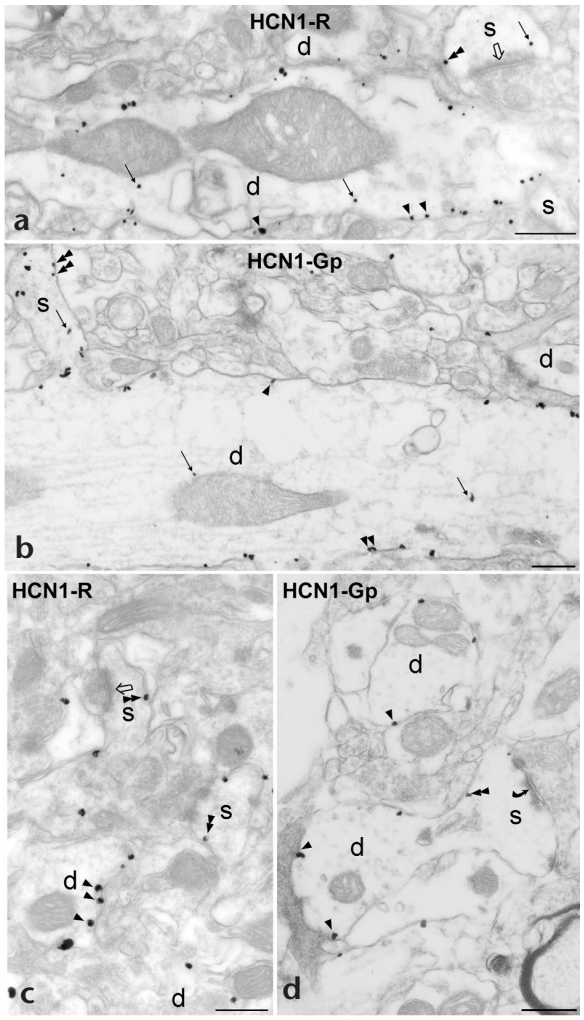

Fig. 4. Electron-microscopic immunogold localization of HCN1 immunoreactivity. Neocortex (**a**, **b**) and hippocampal CA1 (**c**, **d**) are labeled with HCN1-R (**a**, **c**) and HCN1-Gp (**b**, **d**) antibodies. (**a**, **b**) Most gold particles labeling HCN1 are found along dendritic (d) plasma membranes (arrowheads), presumably originating from layer-5 pyramidal cells. Gold particles (double arrowheads) are also attached to the plasma membrane of dendritic spines (s). Some particles are present in the cytoplasm of dendrites and spines (small arrows). No gold particle is associated with an asymmetric synapse (open arrow) or seen over mitochondria. (**c**, **d**) A similar pattern of gold particle distribution was found in the stratum lacunosum-moleculare of hippocampal CA1. The plasma membranes of pyramidal cell apical dendrites (d) are strongly labeled (arrowheads). Fewer particles are associated with spine membranes (double arrowheads). The density of immunogold particles was similar in the apical dendrites of layer 5 and CA1 pyramidal cells, but was lower than that in subicular pyramidal cells. Note that immunogold particles are mainly present on the cytoplasmic side of the dendritic plasma membrane (arrowheads). Images in (**a**, **c**) and (**b**, **d**) from rats perfused with fixatives containing 0.05% and 1% glutaraldehyde, respectively. Scale bars, (**a**, **b**) 0.4 μm; (**c**, **d**) 0.2 μm.

However, the somata and proximal dendrites of CA1 pyramidal cells were mainly immunonegative with the immunogold method, similar to layer-5 cells. The strongest immunolabeling was observed in the subiculum at the LM level, so we turned to this region to investigate the subcellular distribution of HCN1. Indeed, a much higher gold particle density was found in the apical dendrites of subicular pyramidal cells in stratum moleculare than the apical tufts of CA1 and layer-5 pyramidal cells (**Figs. 4** and **5a**, **b** and **e**). In the subiculum, the somatic and proximal dendritic membranes also contained a few gold particles (**Fig. 5c**, **d**, **f** and **g**), but their density seemed to be higher than expected from random, nonspecific labeling. As in the CA1 area and the neocortex, it was immediately apparent that the density of gold particles was much higher at distal dendrites and spines than on the somata and proximal dendritic shafts and spines. To determine which subcellular compartments contain significant amounts of immunoreactive HCN1 and to estimate the difference in the density of HCN1 in distal and proximal plasma membranes, we quantitatively evaluated the immunogold reactions in the subiculum (Methods).

Quantitative analysis of HCN1 immunogold labeling

First, we calculated the nonspecific labeling density in every reaction over the nuclei of pyramidal cells, a subcellular compartment, which should not contain any HCN1. The immunoparticle densities over the nuclei were 0.44 ± 0.26 particles/μm^2 (585 ± 121 μm^2 measured in each animal, $n = 5$ rats) and 0.01 ± 0.01 particles/μm^2 (490 ± 160 μm^2 measured, $n = 3$ rats) for the reactions obtained with the HCN1-R and HCN1-Gp antibodies, respectively. Then we asked which proximal and distal subcellular compartments of pyramidal cells contain HCN1 immunogold density significantly higher than the background, nonspecific density. Nine of ten studied subcellular compartments had HCN1 density above background; only the gold particle density of proximal spine cytoplasm did not differ significantly from that obtained over the nuclei (**Fig. 6b** and **c**; **Table 1**). Immunogold in the cytoplasm may represent channels being transported to or from the plasma membranes. We often detected gold particles associated with somatic endoplasmic reticulum (**Fig. 5d** and **g**) and Golgi apparatus, rendering the somatic cytoplasmic compartment also a substantial pool. The somatic cytoplasm is much larger than the effective somatic plasma membrane; therefore, even at a lower cytoplasmic HCN1 gold density (HCN1-R, 0.23 gold/μm^2 versus 0.38 gold/μm^2; HCN1-Gp, 0.13 gold/μm^2 versus 0.47 gold/μm^2 after nonspecific labeling subtraction), the total number of gold particles could be significantly larger in the cytoplasm. We calculated the mean proportion of gold particles in the somatic cytoplasm to be 91.3 ± 4.8% of the total somatic gold particles. The cytoplasmic pool at distal dendritic and spine compartments (29.1 ± 5.1% and 29.0 ± 12.0%, respectively) was much smaller than at the somatic level.

To determine the differences in density between distinct proximal and distal plasma membrane compartments of pyramidal cells, we compared immunoparticle densities in plasma membrane compartments that had significant amounts of HCN1 labeling (**Fig. 6b** and **c**, insets; **Table 1**). The density of immunoreactive HCN1 was ~70 and 55 times higher ($P < 0.01$ ANOVA; $P < 0.05$ paired comparisons with Tukey correction) in distal dendritic plasma membranes than in somatic membranes for the HCN1-R and HCN1-Gp antibodies, respectively. The 13- and 25-fold difference between proximal and distal dendrites for the HCN1-R and HCN1-Gp antibodies, respectively, was not the consequence of differences in the diameter of the dendrites, as we selected small-diameter proximal dendrites and found their density very similar to that of large-diameter proximal apical dendrites. These results demonstrate a distance-dependent increase

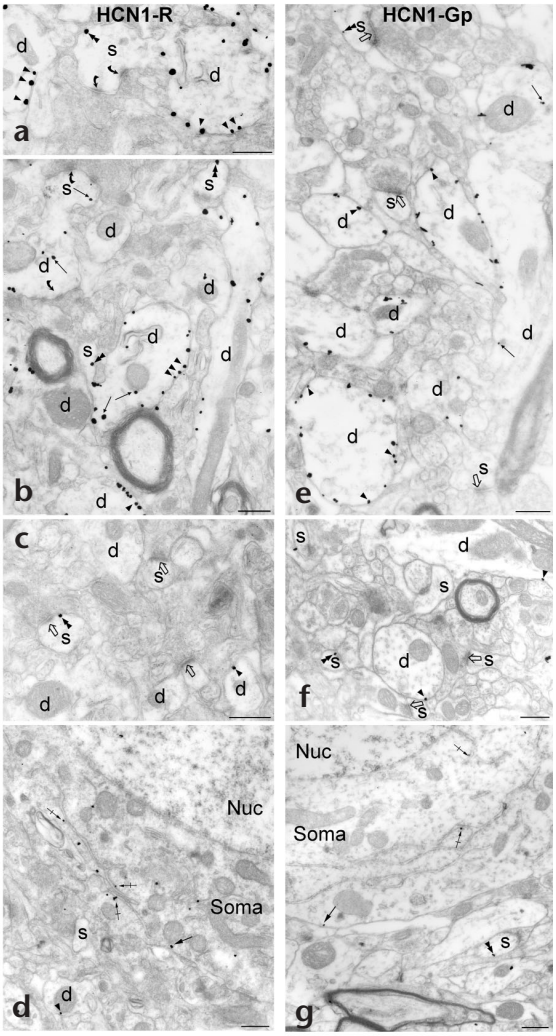

Fig. 5. Electron micrographs showing the subcellular distribution of HCN1 immunoreactivity in the subiculum. (**a**–**d**) HCN1-R antibody. (**e**–**g**) HCN1-Gp antibody. (**a**, **b**, **e**) In stratum moleculare, very strong labeling (arrowheads) is found in the dendritic (d) plasma membranes and a lower particle density is observed in spine (s) membranes (double arrowheads). Some particles are also seen in the cytoplasm (small arrows). No immunoparticle is associated with asymmetrical synapses (open arrows; perforated synapses, curved arrows). (**c**, **f**) Proximal dendritic shafts (arrowheads) and spine (double arrowheads) have a much lower density of plasma membrane labeling than those located in the stratum moleculare. (**d**, **g**) Gold particle density is similarly low in the somatic plasma membrane (arrows). Few immunoparticles are detected in the somatic cytoplasm, some of which are clearly associated with the membrane of the endoplasmic reticulum (crossed arrows). The nucleus (nuc) contains very few particles. Images in (**a**–**d**) and (**e**–**g**) from rats perfused with fixatives containing 0.05% and 1% glutaraldehyde, respectively. Scale bars, 0.4 μm.

in the surface density of HCN1 on the somatodendritic domains of subicular pyramidal cells. However, when the density of immunoreactive HCN1 was compared in the stratum moleculare, we found 3.3 and 4.3 times higher ($P < 0.05$ paired comparision with Tukey correction) values in distal dendritic shafts than in spines for the HCN1-R and HCN1-Gp antibodies, respectively. This finding establishes that not only the distance from the soma, but the actual subcellular domain are important in determining the surface density of HCN1.

Discussion

Our findings using high-resolution immunolocalization of HCN1 in neocortical, hippocampal and subicular pyramidal cells demonstrate the uneven axo-somato-dendritic distribution of a voltage-gated ion channel. Pyramidal cell axon initial segments, small-diameter axons and axon terminals had an undetectable level of HCN1, whereas somata and proximal and distal dendrites expressed significant amounts of HCN1 (domain dependence). Distal dendritic shafts and spines had significantly higher density of HCN1 than proximal shafts and spines of similar diameters, demonstrating that the density of HCN1 increases as a function of distance from the soma (distance dependence). Furthermore, distal dendritic shafts had significantly higher density of HCN1 labeling than did spines at the same average distance from the soma, revealing the subcellular compartment–specific regulation of HCN1 surface density (subcellular compartment dependence). These results establish some new rules in the subcellular distribution of voltage-gated ion channels on the surface of nerve cells and demonstrate that the cell-surface distribution of voltage-gated ion channels is as complex and highly regulated as that of ligand-gated channels.

HCN1 is not the only HCN subunit in the CNS. Four subunits (HCN1–4) have been identified so far[35–38], with distinct distribution and functional properties. The homo- or heteromeric assemblies of these subunits are mainly responsible for the functional diversities of I_h[39,40]. The HCN3 and 4 subunits have an undetectably low level of expression in the hippocampus and the neocortex, but HCN2 is strongly expressed in hippocampal as well as neocortical pyramidal cells[43,44]. The subcellular distribution of HCN2 in pyramidal cells is similar to that of HCN1 as observed at the light microscopic level (A.L., T.N., R.S. and Z.N., unpub. data), suggesting that the organization of the cell surface distribution of HCN1 described in this study is likely to be the same for I_h.

The surface of cortical and hippocampal pyramidal cells is subdivided by incoming excitatory and inhibitory inputs[45,46]. For example, in CA1, entorhinal inputs terminate in the stratum lacunosum-moleculare and innervate the distal apical tufts of pyramidal cells. Schaffer collaterals innervate the strata oriens and radiatum, and the local axon collaterals of CA1 pyramidal cells mainly form synapses in the stratum oriens. Similar to the excitatory inputs, the local circuit inhibitory interneurons also provide spatially segregated GABAergic inputs to subicular, hippocampal and neocortical pyramidal cells. Thus, one possibility for the observed gradient in HCN1 density is that presynaptic excitatory and/or inhibitory synaptic inputs influence the density of HCN1 in the postsynaptic plasma membrane. Another possibility may be that the postsynaptic cell provides the cues for the uneven HCN1 densities in a distance- and subcellular compartment–dependent manner. The finding that there is a clear increase in the HCN1 density within stratum radiatum in the hippocampal CA1 area as a function of distance from the stratum pyramidale indicates that the first possibility may not be the case. However, to unequivocally distinguish between the above two possibilities, the location of the presynaptic inputs should be systematically altered (for instance, using genetic approaches), and its effect on the HCN1 densities should be analyzed.

Irrespective of whether the presynaptic inputs are the primary determinants of the uneven HCN1 densities or not, distal

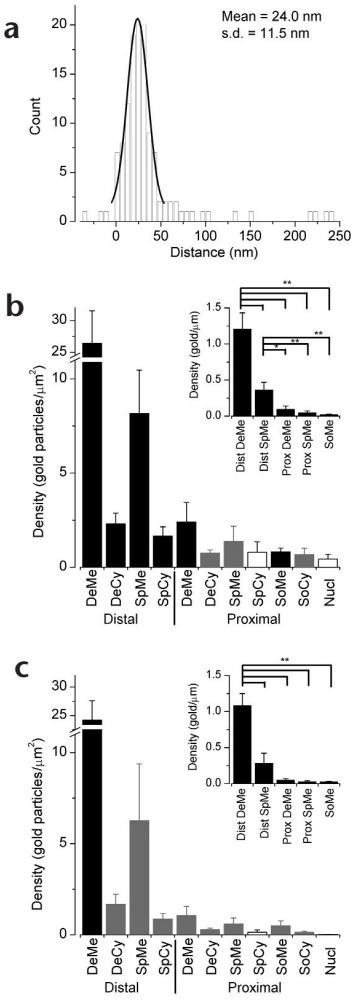

Fig. 6. Quantitative evaluation of immunogold distribution of HCN1 in subicular pyramidal cells. (**a**) Histogram showing the radial distribution of gold particles (HCN1-R) around dendritic plasma membranes. Values along *x*-axis represent the distance from the center of the gold particle to the center of the plasma membrane (positive sign indicates cytoplasmic side; negative sign, extracellular side of the membrane). Bin width, 6 nm. The best Gaussian fit to the data had a peak position at 24 nm on the cytoplasmic side of the membrane and s.d. of 11.5 nm. (**b**, **c**) Quantitative comparison of immunoreactive HCN1 densities obtained with HCN1-R (**b**) and HCN1-Gp (**c**) antibodies in different subcellular compartments of subicular pyramidal cells. Immunoparticle densities (in 'particle per area', Methods) are compared in different proximal and distal subcellular compartments (DeMe, dendritic plasma membrane; DeCy, dendritic cytoplasm; SpMe, spine plasma membrane; SpCy, spine cytoplasm; SoMe, somatic plasma membrane; SoCy, somatic cytoplasm) to the nonspecific labeling density determined over nuclei (nucl). A significant (black bars, $P < 0.01$; gray bars: $P < 0.05$; paired *t*-test) pool of immunoreactive HCN1 was found in all but one (proximal spine cytoplasm) of the subcellular compartments. Insets, immunogold particle density (in 'particle per cut membrane length') in plasma membrane compartments. $P < 0.0001$ ANOVA, $^{**}P < 0.01$, $^{*}P < 0.05$ paired comparisons using Tukey correction. Data given as mean ± s.d.

synaptic inputs will locally interact with a higher density of I_h than their proximally terminating counterparts. The uneven distribution of I_h in pyramidal cell somato-dendritic surface has been observed with patch-clamp and imaging techniques[25–31], in line with our results. Here we provide evidence that the augmented I_h is indeed the consequence of an increased HCN1 channel density. Furthermore, by using a high-resolution EM technique, we were able to examine the HCN1 densities in compartments (small-caliber secondary and tertiary dendrites and spines) that are inaccessible to patch-clamp methods. By comparing the HCN1 labeling densities in small-caliber distal dendrites and in somata, we found a 60-fold difference, much larger than the 7-fold difference found on CA1 pyramidal cells with patch-clamp recordings[25]. Although we were unable to quantitatively determine how the HCN1 density increases as a function of distance on the apical dendrites of pyramidal cells, we had the impression that the distance-dependent increase in HCN1 density is not linear.

The uneven HCN1 densities on pyramidal cell dendrites may have several functional consequences[26–30]. It is suggested that the increased I_h could contribute to the distance-independent temporal summation of excitatory postsynaptic potentials (EPSPs)[26,30]. In addition, the somatic EPSP time course is independent of the site of generation of the synaptic potential in layer-5 cortical pyramidal cells, and this independence requires I_h[27]. Uneven I_h could also determine the extent to which regenerative events are generated in dendrites and how sub- and

Table 1. Immunoparticle densities for HCN1 in distinct subcellular compartments of subicular pyramidal cells.

	HCN1-R (*n* = 5 rats)				HCN1-Gp (*n* = 3 rats)				HCN1-R (*n* = 5 rats)				HCN1-Gp (*n* = 3 rats)			
	Density (gold/μm²)		Measured area (μm²)		Density (gold/μm²)		Measured area (μm²)		Density (gold/μm)		Measured length (μm)		Density (gold/μm)		Measured length (μm)	
	Mean	s.d.	Mean	s.d.	Mean	s.d.	Mean	s.d.	Mean	s.d.	Mean	s.d.	Mean	s.d.	Mean	s.d.
Dist DeMe	***26.66***	4.89	10.2	2.1	***23.46***	3.70	8.7	0.5	1.206	0.225	222.4	45.7	1.079	0.170	190.0	10.2
Dist DeCy	**2.32**	0.58	55.6	13.3	**1.64**	0.54	58.7	7.9								
Dist SpMe	***8.24***	2.32	4.1	0.3	**6.12**	3.04	3.7	0.7	0.359	0.107	89.3	6.3	0.281	0.140	80.8	15.8
Dist SpCy	***1.67***	0.50	11.2	1.7	**0.84**	0.31	9.7	2.8								
Prox DeMe	**2.42**	1.05	7.5	1.4	**1.03**	0.49	7.7	0.9	0.091	0.048	162.9	31.3	0.047	0.022	166.5	19.0
Prox DeCy	**0.76**	0.16	37.9	11.3	**0.27**	0.09	47.1	4.9								
Prox SpMe	**1.38**	0.80	4.7	1.3	**0.58**	0.32	3.5	0.2	0.043	0.027	95.6	14.6	0.026	0.015	75.8	4.9
Prox SpCy	0.80	0.56	10.2	1.5	0.14	0.13	6.9	1.0								
SoMe	***0.82***	0.21	21.7	2.1	**0.48**	0.27	15.5	4.0	0.017	0.010	472.8	45.9	0.022	0.012	336.2	86.7
SoCy	**0.67**	0.34	637.1	114.8	**0.14**	0.06	592.3	300.3								
Nucleus	0.44	0.26	584.9	121.3	0.01	0.01	490.4	160.1								

Bold, $P < 0.05$; bold and italic, $P < 0.01$; paired *t*-test. DeMe, dendritic plasma membrane; DeCy, dendritic cytoplasm; SpMe, spine plasma membrane; SpCy, spine cytoplasm; SoMe, somatic plasma membrane; SoCy, somatic cytoplasm.

suprathreshold events propagate to the soma[28–30]. It will be interesting to see how the uneven somatodendritic I_h influences the time course and temporal summation of hyperpolarizing inhibitory postsynaptic potentials originating from different types of interneurons innervating distinct compartments of the postsynaptic pyramidal cell.

We also observed a significant difference in HCN1 density between the plasma membrane of dendritic shafts and spines. The lower HCN1 density in spines may indicate that the activation/inactivation of I_h may not be synapse specific, but several presynaptic cells converging onto the same dendritic segment may jointly use the high I_h density in small-diameter dendrites. The relatively slow time course of I_h kinetics suggests that coincident activation of distal synapses may not be required for their activation, and I_h activated by preceding synaptic activity could selectively alter the efficacy and summation properties of neighboring, distal synapses. Moreover, synapses targeting the spines would be less influenced by local I_h activation than inputs located on dendritic shafts. Because most GABAergic synapses target dendritic shafts and glutamatergic synapses terminate on the spines, this scenario suggests a preferential activation of I_h by GABAergic inputs. Another possibility is that the difference between the HCN1 density in dendritic shafts and spines may reflect an adaptation to an uneven distribution of some regulatory processes, which requires the close spatial colocalization of the regulatory proteins (such as G-protein-coupled receptors) and the effector HCN channels. Future studies may test these predictions experimentally.

Methods

Antibody preparation. We developed a guinea pig polyclonal antibody (N12) against a glutathione S-transferase fusion protein containing the C-terminus of rat HCN1 (amino acid residues 850–910) using a described method[47]. The fusion protein was purified by preparative sodium dodecyl sulfate–polyacrylamide gel electrophoresis (SDS-PAGE) for immunization. Excised gels containing the purified fusion protein were emulsified with Freund's complete adjuvant (Nacalai tesque, Kyoto, Japan) and injected subcutaneously into guinea pigs (50–100 μg fusion protein per animal). After 4 weeks, the fusion protein was injected again with Freund's incomplete adjuvant. From antisera collected 2 weeks after the second injection, HCN1 antibody was affinity purified using a CNBr-activated glutathione Sepharose 4B (Amersham Pharmacia Biotech, Upsala, Sweden) coupled to the purified fusion protein. The rabbit polyclonal antibody to HCN1 was purchased from Alomone Labs (Jerusalem, Israel) and was raised against the N-terminus of the rat HCN1 (amino acid residues 6–24).

Immunoblotting. Crude membrane fractions of the whole brain were prepared from adult male rats (Sprague–Dawley, Charles River, Japan) as described[47]. The membrane fractions were separated by 7.5% SDS-PAGE and transferred to nitrocellulose membranes (Bio-Rad, Hercules, California, USA). The membranes were blocked with Block-Ace (Dainippon Pharmaceutical, Suita, Japan) and then reacted with the rabbit (0.5 μg/ml) and guinea pig (0.2 μg/ml) HCN1 antibodies. An alkaline phosphatase–labeled secondary antibody (Chemicon, Temecula, California, USA) was used to visualize the reactions. The immunoreactivity completely disappeared after preincubation of these antibodies with the respective antigens, indicating that both antibodies specifically react with rat HCN1 (**Fig. 1**).

Preparation of tissue for immunocytochemistry. Sixteen adult (P35–67) male Wistar rats were deeply anesthetized with ketamine (30 mg/kg) and xylazine (10 mg/kg) in accordance with the guidelines of the Institute of Experimental Medicine Protection of Research Subjects. Twelve rats were perfused through the aorta with 0.9% saline for 1 min, followed by ice-cold fixatives, containing 4% paraformaldehyde, 0.05% glutaraldehyde, and 15% (v/v) picric acid made up in 0.1 M phosphate buffer (PB, pH 7.4) for 11–30 min for light and electron microscopy. An additional rat was perfused with a fixative containing 4% paraformaldehyde and 15% (v/v) picric acid in PB for light microscopy. The brains were immediately removed, and blocks were cut out from the forebrain and kept in 0.1 M PB. Three animals were perfused first with 0.9% saline for 1 min, followed by a fixative containing 4% paraformaldehyde and 1% glutaraldehyde in 0.1 M sodium acetate buffer (pH = 6.0) for 2 min, followed by an hour fixation with a fixative containing 4% paraformaldehyde and 1% glutaraldehyde in 0.1 M sodium borate buffer (pH 8.0)[48] for EM analysis. After the perfusion, the brains were left in the skull for 24 h at 4°C. The brains were then removed, and horizontal sections (60 μm thick) were prepared with a Vibratome (VT1000S, Leica Microsystems, Vienna, Austria), then collected and washed several times in 0.1 M PB.

Pre-embedding immunocytochemistry. Normal goat serum (NGS, 10%) in Tris-buffered saline (TBS, pH 7.4) was used for blocking, followed by incubations in the primary and secondary antibodies as described[42]. Briefly, rabbit and guinea pig antibodies to HCN1 were diluted in TBS containing 2% NGS and 0.05% Triton X-100 at final concentrations of 2–4 μg/ml and 1.4 μg/ml, respectively. Sections for fluorescence double-labeling experiments were further incubated in the mixture of Alexa-594-conjugated goat anti-rabbit IgG (1:500, Molecular Probes, Leiden, The Netherlands; diluted in TBS containing 2% NGS) and biotinylated goat anti–guinea pig IgG (Vector Laboratories, Burlingame, California; diluted 1:50) for 3 h. Following several washes, the sections were incubated in avidin-biotinylated HRP complex (ABC, Vector Laboratories) for 2 h followed by a tiramid–Oregon green (Molecular Probes) reaction as described by the manufacturer. After several washes in buffer, the sections were mounted on slides in Vectashield (Vector Laboratories). Sections for immunoperoxidase reactions were incubated in biotinylated goat anti-rabbit and goat anti–guinea pig IgGs (Vector Laboratories; diluted 1:50 in TBS containing 2% NGS) for 3 h, followed by several washes, and an incubation in ABC for 2 h. The enzyme reaction was revealed by 3′3-diaminobenzidine tetrahydrochloride (0.05%) as chromogen and 0.01% H_2O_2 as oxidant. Sections for the immunogold reaction were incubated in goat anti-rabbit and goat anti–guinea pig IgGs coupled to 0.8-nm gold particles (Aurion Immunoresearch, Wageningen, The Netherlands; diluted 1:50 in TBS containing 2% NGS). The UltraSmall gold particles were silver enhanced using R-Gent SE-LM Silver kit as described by the manufacturer (Aurion). For light microscopy, sections were mounted on gelatin-coated slides, dried, dehydrated and embedded in DePeX mounting medium (Electron Microscopy Sciences, Washington, Pennsylvania). Sections for electron microscopy were postfixed with 0.5–1% OsO_4, contrasted in 1% uranyl acetate, dehydrated in graded alcohol series, and embedded into epoxy resin (Durcupan, Fluka, Buchs, Switzerland). No specific immunoreactivity could be detected when either the primary or the secondary or both antibodies were omitted and the sections were treated with the silver kit.

Quantitative analysis of the immunogold reactions. As the light microscopic distribution and the qualitative pattern of HCN1 immunogold distribution was almost the same in layer 5, hippocampal CA1 and subicular pyramidal cells, we chose subicular pyramidal cells to quantitatively evaluate the relative densities of HCN1 in distinct subcellular compartments because the strongest immunolabeling was observed in the subiculum, giving the highest signal-to-noise ratio. The highest possible signal is essential for revealing all subcellular compartments with significant amounts of immunoreactive HCN1. The disadvantage of choosing subicular compared to CA1 pyramidal cells is that the pyramidal cell bodies are not arranged in a well-defined layer in the subiculum. Thus, the distance of a dendrite from the soma cannot be easily determined from its location. Consequently, we focused our attention to the following distal and proximal subcellular compartments: distal dendritic plasma membranes, dendritic cytoplasm, distal spine membranes, spine cytoplasm, proximal dendritic plasma membranes, dendritic cytoplasm, proximal spine membranes, spine cytoplasm, somatic plasma membranes, somatic cytoplasm. We calculated the nonspecific immunoparticle density over pyramidal cell nuclei, as this compart-

ment should not contain any HCN1. Samples representing proximal dendrites and spines were taken from regions adjacent to the somata of pyramidal cells located close to the alveus (deep layers). Samples representing the distal part of apical dendrites and spines were taken from the stratum moleculare. Electron micrographs were taken within the same ultrathin section from randomly selected fields in stratum moleculare (30.2 ± 7.5 images per animal) and in deep subicular layers (27.5 ± 9 images per animal). Parts of a pyramidal cell soma were reconstructed from an average of 23 micrographs in 2–4 serial sections. A total of 31 pyramidal cell somata is included in the study. Special care was taken that the ultrathin sections contained tissue from the same depth, and reactions were only compared within the same depth. Reactions, obtained with the rabbit antibody at 3, 4.5 and 6 μm depths, were analyzed. Both specific and nonspecific immunoparticle density decreased as a function of depth into the tissue. Thus, we concluded that specific immunoparticle densities could only be compared within the same depth of the tissue. The highest signal-to-noise ratio was found at 3 μm depth from the surface; therefore all data in the manuscript were acquired at this depth. For reactions obtained with the guinea pig antibody, all measurements were made at the surface of the tissue (within the first μm) because nonspecific labeling density was virtually zero over the nuclei already at this depth.

In each electron micrograph, dendritic shafts and spines and pyramidal somata were identified, and gold particles were counted in their cytoplasm as well as on the plasma membranes. Pyramidal cell dendrites were identified from the lack of asymmetrical synapses on the shaft; they may receive symmetrical synapses, and they usually contained mitochondria. Spines were identified as receiving asymmetrical synapses and from the lack of mitochondria. Both labeled and unlabeled profiles were included in the analysis. We have measured the distances of gold particles from the plasma membranes (from the middle of the membrane to the middle of the particle) and analyzed their distribution. A Gaussian distribution provided an adequate fit to the data with a peak location of 24 nm from the membrane and an s.d. of 11.5 nm (**Fig. 6a**). We have considered a gold particle to be associated with the plasma membrane if it was within 46 nm from the cytoplasmic side of the membrane (± 2× s.d. around the mean), resulting in an effective membrane width of 46 nm. The immunoparticle density was calculated in particle/effective membrane area in an EM picture (in particle/μm^2) over all plasma membrane compartments and was statistically compared to the nonspecific labeling densities (also given in particle/μm^2) with the paired *t*-test. Membrane lengths (in μm) and areas (in μm^2) were measured with Scion Image 4.0.2 (2000 Scion Corporation, Bethesda, Maryland). Immunoparticle densities for somatic, dendritic and spine cytoplasm were also calculated in particle/area (particle/μm^2) and were statistically compared to the nonspecific labeling density with a paired *t*-test. For those plasma membrane compartments that contained significant amounts of immunoreactive HCN1 (**Fig. 6b** and **c**), we also calculated immunoparticle densities in particle per cut membrane length following nonspecific labeling subtraction (**Fig. 6b** and **c**, insets). Data are given as mean ± s.d.

Acknowledgments

Z.N. received grants from the Hungarian Science Foundation (T032309), the Howard Hughes Medical Institute, the James S. McDonnell Foundation, the Wellcome Trust and the Boehringer Ingelheim Fund. Z.N. and R.S. received grants from CREST—Japan Science and Technology Corporation. G.T. is funded by the Wellcome Trust.

Competing interests statement

The authors declare that they have no competing financial interests.

RECEIVED 27 AUGUST; ACCEPTED 1 OCTOBER 2002

1. Hille, B. *Ionic Channels of Excitable Membranes* (Sinauer, Sunderland, Massachusetts, 2001).
2. Conti, F. & Weinberg, R. J. Shaping excitation at glutamatergic synapses. *Trends Neurosci.* **22**, 451–458 (1999).
3. Ottersen, O. P. & Landsend, A. S. Organization of glutamate receptors at the synapse. *Eur. J. Neurosci.* **9**, 2219–2224 (1997).
4. Somogyi, P., Nusser, Z., Roberts, J. D. B. & Lujan, R. in *Precision and Variability in the Placement of Pre- and Postsynaptic Receptors in Relation to Neurotransmitter Release Sites* 82–93 (HFSP, Strasbourg, 1998).
5. Yuste, R. & Tank, D. W. Dendritic integration in mammalian neurons, a century after Cajal. *Neuron* **16**, 701–716 (1996).
6. Craig, A. M. & Boudin, H. Molecular heterogeneity of central synapses: afferent and target regulation. *Nat. Neurosci.* **4**, 569–578 (2001).
7. Petralia, R. S., Rubio, M. E. & Wenthold, R. J. Selectivity in the distribution of glutamate receptors in neurons. *Cell. Biol. Int.* **22**, 603–608 (1998).
8. Magee, J., Hoffman, D., Colbert, C. & Johnston, D. Electrical and calcium signaling in dendrites of hippocampal pyramidal neurons. *Annu. Rev. Physiol.* **60**, 327–346 (1998).
9. Rubio, M. E. & Wenthold, R. J. Glutamate receptors are selectively targeted to postsynaptic sites in neurons. *Neuron* **18**, 939–950 (1997).
10. Nusser, Z. *et al.* Cell type and pathway dependence of synaptic AMPA receptor number and variability in the hippocampus. *Neuron* **21**, 545–559 (1998).
11. Takumi, Y., Ramirez-Leon, V., Laake, P., Rinvik, E. & Ottersen, O. P. Different modes of expression of AMPA and NMDA receptors in hippocampal synapses. *Nat. Neurosci.* **2**, 618–624 (1999).
12. Fritschy, J.-M., Weinmann, O., Wenzel, A. & Benke, D. Synapse-specific localization of NMDA and $GABA_A$ receptor subunits revealed by antigen-retrieval immunohistochemistry. *J. Comp. Neurol.* **390**, 194–210 (1998).
13. Watanabe, M. *et al.* Selective scarcity of NMDA receptor channel subunits in the stratum lucidum (mossy fibre-recipient layer) of the mouse hippocampal CA3 subfield. *Eur. J. Neurosci.* **10**, 478–487 (1998).
14. Nusser, Z., Sieghart, W., Benke, D., Fritschy, J.-M. & Somogyi, P. Differential synaptic localization of two major γ-aminobutyric acid type A receptor α subunits on hippocampal pyramidal cells. *Proc. Natl. Acad. Sci. USA* **93**, 11939–11944 (1996).
15. Nyiri, G., Freund, T. F. & Somogyi, P. Imput-dependent synaptic targeting of α2-subunit-containing $GABA_A$ receptors in synapses of hippocampal pyramidal cells of the rat. *Eur. J. Neurosci.* **13**, 428–442 (2001).
16. Nusser, Z., Cull-Candy, S. G. & Farrant, M. Differences in synaptic $GABA_A$ receptor number underlie variation in GABA mini amplitude. *Neuron* **19**, 697–709 (1997).
17. Nusser, Z., Hajos, N., Somogyi, P. & Mody, I. Increased number of synaptic $GABA_A$ receptors underlies potentiation at hippocampal inhibitory synapses. *Nature* **395**, 172–177 (1998).
18. Nusser, Z., Sieghart, W. & Somogyi, P. Segregation of different $GABA_A$ receptors to synaptic and extrasynaptic membranes of cerebellar granule cells. *J. Neurosci.* **18**, 1693–1703 (1998).
19. Hu, H. *et al.* Presynaptic Ca^{2+}-activated K^+ channels in glutamatergic hippocampal terminals and their role in spike repolarization and regulation of transmitter release. *J. Neurosci.* **21**, 9585–9597 (2001).
20. Hoffman, D. A., Magee, J. C., Colbert, C. M. & Johnston, D. K^+ channel regulation of signal propagation in dendrites of hippocampal pyramidal neurons. *Nature* **387**, 869–875 (1997).
21. Bischofberger, J. & Schild, D. Different spatial patterns of $[Ca^{2+}]$ increase caused by N- and L-type Ca^{2+} channel activation in frog olfactory bulb neurones. *J. Physiol. (Lond.)* **487**, 305–317 (1995).
22. Christie, B. R., Eliot, L. S., Ito, K., Miyakawa, H. & Johnston, D. Different Ca^{2+} channels in soma and dendrites of hippocampal pyramidal neurons mediate spike-induced Ca^{2+} influx. *J. Neurophysiol.* **73**, 2553–2557 (1995).
23. Stuart, G. & Hausser, M. Initiation and spread of sodium action potentials in cerebellar Purkinje cells. *Neuron* **13**, 703–712 (1994).
24. Magee, J. C. & Johnston, D. Characterization of single voltage-gated Na^+ and Ca^{2+} channels in apical dendrites of rat CA1 pyramidal neurons. *J. Physiol. (Lond.)* **487**, 67–90 (1995).
25. Magee, J. C. Dendritic hyperpolarization-activated currents modify the integrative properties of hippocampal CA1 pyramidal neurons. *J. Neurosci.* **18**, 7613–7624 (1998).
26. Magee, J. C. Dendritic I_h normalizes temporal summation in hippocampal CA1 neurons. *Nat. Neurosci.* **2**, 508–514 (1999).
27. Williams, S. R. & Stuart, G. J. Site independence of EPSP time course is mediated by dendritic I_h in neocortical pyramidal neurons. *J. Neurophysiol.* **83**, 3177–3182 (2000).
28. Stuart, G. & Spruston, N. Determinants of voltage attenuation in neocortical pyramidal neuron dendrites. *J. Neurosci.* **18**, 3501–3510 (1998).
29. Schwindt, P. C. & Crill, W. E. Modification of current transmitted from apical dendrite to soma by blockade of voltage- and Ca^{2+}-dependent conductances in rat neocortical pyramidal neurons. *J. Neurophysiol.* **78**, 187–198 (1997).
30. Berger, T., Larkum, M. E. & Luscher, H. R. High I_h channel density in the distal apical dendrite of layer V pyramidal cells increases bidirectional attenuation of EPSPs. *J. Neurophysiol.* **85**, 855–868 (2001).
31. Tsubokawa, H., Miura, M. & Kano, M. Elevation of intracellular Na^+ induced by hyperpolarization at the dendrites of pyramidal neurones of mouse hippocampus. *J. Physiol. (Lond.)* **517**, 135–142 (1999).
32. Stuart, G. J. & Sakmann, B. Active propagation of somatic action potentials into neocortical pyramidal cell dendrites. *Nature* **367**, 69–72 (1994).
33. Colbert, C. M. & Johnston, D. Axonal action-potential initiation and Na^+ channel densities in the soma and axon initial segment of subicular pyramidal neurons. *J. Neurosci.* **16**, 6676–6686 (1996).
34. Hoffman, D. A. & Johnston, D. Downregulation of transient K^+ channels in dendrites of hippocampal CA1 pyramidal neurons by activation of PKA and PKC. *J. Neurosci.* **18**, 3521–3528 (1998).
35. Gauss, R., Seifert, R. & Kaupp, U. B. Molecular identification of a

hyperpolarization-activated channel in sea urchin sperm. *Nature* **393**, 583–587 (1998).
36. Santoro, B., Grant, S. G., Bartsch, D. & Kandel, E. R. Interactive cloning with the SH3 domain of N-src identifies a new brain specific ion channel protein, with homology to eag and cyclic nucleotide-gated channels. *Proc. Natl. Acad. Sci. USA* **94**, 14815–14820 (1997).
37. Monteggia, L. M., Eisch, A. J., Tang, M. D., Kaczmarek, L. K. & Nestler, E. J. Cloning and localization of the hyperpolarization-activated cyclic nucleotide-gated channel family in rat brain. *Brain Res. Mol. Brain Res.* **81**, 129–139 (2000).
38. Ludwig, A., Zong, X., Jeglitsch, M., Hofmann, F. & Biel, M. A family of hyperpolarization-activated mammalian cation channels. *Nature* **393**, 587–591 (1998).
39. Chen, S., Wang, J. & Siegelbaum, S. A. Properties of hyperpolarization-activated pacemaker current defined by coassembly of HCN1 and HCN2 subunits and basal modulation by cyclic nucleotide. *J. Gen. Physiol.* **117**, 491–504 (2001).
40. Seifert, R. *et al.* Molecular characterization of a slowly gating human hyperpolarization-activated channel predominantly expressed in thalamus, heart, and testis. *Proc. Natl. Acad. Sci. USA* **96**, 9391–9396 (1999).
41. Baude, A., Nusser, Z., Molnar, E., McIlhinney, R. A. & Somogyi, P. High-resolution immunogold localization of AMPA type glutamate receptor subunits at synaptic and non-synaptic sites in rat hippocampus. *Neuroscience* **69**, 1031–1055 (1995).
42. Nusser, Z. *et al.* Immunocytochemical localization of the α1 and β2/3 subunits of the $GABA_A$ receptor in relation to specific GABAergic synapses in the dentate gyrus. *Eur. J. Neurosci.* **7**, 630–646 (1995).
43. Moosmang, S., Biel, M., Hofmann, F. & Ludwig, A. Differential distribution of four hyperpolarization-activated cation channels in mouse brain. *Biol. Chem.* **380**, 975–980 (1999).
44. Bender, R. A. *et al.* Differential and age-dependent expression of hyperpolarization-activated, cyclic nucleotide-gated cation channel isoforms 1-4 suggests evolving roles in the developing rat hippocampus. *Neuroscience* **106**, 689–698 (2001).
45. Freund, T. F. & Buzsaki, G. Interneurons of the hippocampus. *Hippocampus* **6**, 347–470 (1996).
46. Somogyi, P., Tamas, G., Lujan, R. & Buhl, E. H. Salient features of synaptic organisation in the cerebral cortex. *Brain Res. Rev.* **26**, 113–135 (1998).
47. Shigemoto, R. *et al.* Differential presynaptic localization of metabotropic glutamate receptor subtypes in the rat hippocampus. *J. Neurosci.* **17**, 7503–7522 (1997).
48. Sloviter, R. S., Ali-Akbarian, L., Horvath, K. D. & Menkens, K. A. Substance P receptor expression by inhibitory interneurons of the rat hippocampus: enhanced detection using improved immunocytochemical methods for the preservation and colocalization of GABA and other neuronal markers. *J. Comp. Neurol.* 430, 283–305 (2001).